Brank, B., 2008. Assessment of 4-node EAS-ANS shell elements for large deformation analysis. *Comput. mech.*, 42, 1, 39-51.

http://www.springerlink.com/content/l5661k6817320676/fulltext.pdf

DOI: 10.1007/s00466-007-0233-3

Assessment of 4-node EAS-ANS shell elements for large deformation analysis

Boštjan Brank
University of Ljubljana,
Faculty of Civil and Geodetic Engineering, Jamova 2, Ljubljana, Slovenia
e-mail: bbrank@ikpir.fgg.uni-lj.si

November 16, 2007

Abstract

In this work we derive and mutually compare several 4-node shell hyperelastic finite elements for large deformation analysis. The elements are based on Reissner-Mindlin shell theory. They use the enhanced assumed strain (EAS) concept for enhancement of membrane and bending displacement-compatible strains and the assumed natural strain (ANS) concept for treatment of transverse shear strains. The elements differ from each other by the number of membrane and bending EAS parameters. An optimal number of these parameters is suggested on the basis of numerical results.

Key words: shells, finite elements, 4-node element, nonlinear analysis, enhanced assumed strain method, assumed natural strain method

1 Introduction

The enhanced assumed strain (EAS) method, introduced in [23], [24] has been accepted as a relatively simple and efficient tool for performance enhancement of lower order finite elements for linear/nonlinear analysis of solids and structures. The method is closely related to the works on incompatible displacement modes [23].

Since those two initial works many finite elements based on the EAS method have been developed. As concerning shell formulations, the EAS method has been used in two different manners: (i) to obtain *3d-shell* and *solid-shell* formulations that explicitly account for through-the-thickness stretching, and (ii) to obtain classical (i.e. Reissner-Mindlin) shell, 3d-shell and solid shell elements with *improved in-plane* (membrane) performance. Works that go under (i) employ the EAS method to introduce the through-the-thickness stretching in order to derive efficient 3d-shell formulations, e.g. [10], [4], [5], [3], [9], [22], or solid-shell formulations, e.g. [26], [27], [12], [17]. Works that go under (ii) employ the EAS method to improve the in-plane behavior of 3d-shell or solid-shell elements or the membrane behavior of classical (Reissner-Mindlin) shell elements, e.g. [1], [6], [11], and some of the above mentioned 3-shell and solid-shell formulations.

In this paper we focus on EAS enhancement of classical (i.e. Reissner-Mindlin) shell formulations. We are interested in a robust geometrically exact 4-node quadrilateral finite element for nonlinear large rotation analysis that can give good results for coarse and distorted meshes that can arise e.g. in shape optimization problems, e.g. [15], [16]. We study two questions: (i) which is an *optimal number* of EAS parameters for enhancement of membrane/bending strains for 4-node nonlinear geometrically exact shell element, and (ii) does an EAS *enhancement of bending strains* improve performance of that shell element. The interest for the first question comes from the fact that in the recent literature nonlinear 4-node EAS shell elements appear with 4, 5 or 7 enhancement parameters for the improvement of membrane performance, see e.g. [6], [3], [5], [20]. It seems that an optimal number of membrane enhancement parameters has not been considered yet for nonlinear shell elements, although behavior of linear elements with 4 and 7 membrane enhancement parameters is well documented [1]. The interest for the second question comes from the fact that the EAS enhancement of classical shell

formulations has been done exclusively for the membrane strains; there are no formulations avaliable with enhancement of bending strains. We try to answer the above questions on a basis of numerical experience, i.e. by comparing results of a set of characteristic numerical examples for several different membrane/bending EAS formulations. In such a way an optimal number of EAS parameters can be suggested, leading to a low-order shell finite element that allows for accurate and efficient (with coarse and distorted meshes) analysis of shell-like structures undergoing large deformations. The treatment of shear locking problem is in all cases based on the assumed natural strain (ANS) method [2].

As concerning enhancement of the displacement-based strains by using the EAS method, there are basically two approaches: (i) to express the total strains as an additive sum of the displacement-based strains and the enhanced strains [23]; (ii) to perform an enhancement of the deformation gradient [24]. The approach (i) is more suitable for small strain problems because of its additive manner of strain enhancement, while the approach (ii) is more suitable for large strain problems because of a multiplicative manner of strain enhancement. In majority of nonlinear shell, 3-d shell and solid-shell EAS formulations an additive split of strains has been used. This can be justified by the fact that many shell-like structures may undergo large displacements and large rotations while experiencing small strains. Some authors, [4], [9], [27], compared formulations (i) and (ii) for 3d-shell and solid-shell elements and concluded that numerical results based on both approaches are similar for standard examples. Considering the above, the EAS method with an additive sum of strains can be regarded as a suitable tool for derivation of nonlinear shell finite elements. In this work we therefore derive nonlinear shell EAS finite elements with an additive enhancement of strains.

2 Geometrically exact EAS shell formulation

2.1 Geometry, kinematics and strains

We model a shell body as a surface in the 3d space (called midsurface) which has at its every point attached an unextensible unit vector (called shell director). The position vector to a material point in the initial (also called undeformed or reference) stress-free shell configuration is then given by

$$\mathbf{X}\left(\xi^1,\xi^2,\xi\right)=\boldsymbol{\varphi}_0\left(\xi^1,\xi^2\right)+\xi\mathbf{T}\left(\xi^1,\xi^2\right),\qquad \left(\xi^1,\xi^2\right)\in\mathcal{A},\qquad \xi\in\mathcal{F} \tag{1}$$

Here ξ^1 and ξ^2 are convective curvilinear coordinates that parametrize the midsurface $\boldsymbol{\varphi}_0$; $\mathcal{A}$ is the domain of the parametrization; $\mathbf{T}$, $\|\mathbf{T}\|=1$, is the shell director that coincides with the normal vector $\mathbf{N}$ of the midsurface; and ξ is through-the-thickness convected coordinate defined in the domain $\mathcal{F}=[-h/2,h/2]$, where h is initial constant shell thickness. In what follows, we always determine the components of the above vectors with respect to the fixed orthonormal basis $\mathbf{e}_i=\mathbf{e}^i$, $i=1,2,3$, in the 3d space, i.e. $\mathbf{X}=X^i\mathbf{e}_i$, $\boldsymbol{\varphi}_0=\varphi_0^i\mathbf{e}_i$, $\mathbf{T}=T^i\mathbf{e}_i$. We further define the shell director as $\mathbf{T}=\boldsymbol{\Lambda}_0\mathbf{e}_3$, where $\boldsymbol{\Lambda}_0$ is a given (initial) rotation tensor, $\boldsymbol{\Lambda}_0^{-1}=\boldsymbol{\Lambda}_0^T$, $\det\boldsymbol{\Lambda}_0=1$. If one introduces at a midsurface point an orthonormal basis $\widehat{\mathbf{e}}_i=\widehat{\mathbf{e}}^i$ as $\widehat{\mathbf{e}}_3\equiv\mathbf{T}$, the rotation tensor $\boldsymbol{\Lambda}_0$ at that point can be represented as $\boldsymbol{\Lambda}_0=[\widehat{\mathbf{e}}_1,\widehat{\mathbf{e}}_2,\widehat{\mathbf{e}}_3]=[\widehat{\mathbf{e}}_1,\widehat{\mathbf{e}}_2,\mathbf{T}]$.

It is assumed that the position vector in the deformed configuration is given as

$$\mathbf{x}\left(\xi^1,\xi^2,\xi\right)=\underbrace{\left[\boldsymbol{\varphi}_0\left(\xi^1,\xi^2\right)+\mathbf{u}\left(\xi^1,\xi^2\right)\right]}_{\boldsymbol{\varphi}\left(\xi^1,\xi^2\right)}+\xi\mathbf{t}\left(\xi^1,\xi^2\right),\qquad \|\mathbf{t}\|=1 \tag{2}$$

Here $\mathbf{u}$ is the midsurface displacement vector, and $\mathbf{t}$ is the shell director at the deformed configuration, which we choose to be defined by the sequence of two rotations $\mathbf{t}=\boldsymbol{\Lambda}_0\boldsymbol{\Lambda}\mathbf{e}_3$. The components of newly defined vectors in (2) are also determined with respect to the fixed orthonormal basis $\mathbf{e}_i$, i.e. $\mathbf{x}=x^i\mathbf{e}_i$, $\boldsymbol{\varphi}=\varphi^i\mathbf{e}_i$, $\mathbf{u}=u^i\mathbf{e}_i$, and $\mathbf{t}=t^i\mathbf{e}_i$. The rotation tensor $\boldsymbol{\Lambda}$ is viewed in this work as a function of a constrained rotation vector $\boldsymbol{\vartheta}$, i.e. $\boldsymbol{\Lambda}=\widetilde{\boldsymbol{\Lambda}}\left(\boldsymbol{\vartheta}\right)$, [8]. Since the rotation around the shell director (i.e. drilling rotation) plays no role in the present theory, the constrained rotation vector has only two components with respect to the orthonormal basis $\widehat{\mathbf{e}}_i$, i.e. $\boldsymbol{\vartheta}=\vartheta^\alpha\widehat{\mathbf{e}}_\alpha$, $\alpha=1,2$. By using the Rodrigues formula for the representation of the rotation tensor $\widetilde{\boldsymbol{\Lambda}}\left(\boldsymbol{\vartheta}\right)$, one can end up with the following expression $\mathbf{t}=\boldsymbol{\Lambda}_0\left(\cos\vartheta\mathbf{e}_3+\frac{\sin\vartheta}{\vartheta}\boldsymbol{\vartheta}\times\mathbf{e}_3\right)$, $\vartheta=\|\boldsymbol{\vartheta}\|$.

The vectors of the convected basis $\mathbf{G}_i$ at a point of the shell reference configuration are related to the position vector $\mathbf{X}$ and the convected coordinates ξ^α, ξ as

$$\mathbf{G}_\alpha = \frac{\partial \mathbf{X}}{\partial \xi^\alpha} = \frac{\partial \boldsymbol{\varphi}_0}{\partial \xi^\alpha} + \xi \frac{\partial \mathbf{T}}{\partial \xi^\alpha}, \qquad \mathbf{G}_3 = \frac{\partial \mathbf{X}}{\partial \xi} = \mathbf{T} \tag{3}$$

Similarly, the vectors of the convected basis $\mathbf{g}_i$ at the shell deformed configuration are obtained as

$$\mathbf{g}_\alpha = \frac{\partial \mathbf{x}}{\partial \xi^\alpha} = \frac{\partial \boldsymbol{\varphi}}{\partial \xi^\alpha} + \xi \frac{\partial \mathbf{t}}{\partial \xi^\alpha}, \qquad \mathbf{g}_3 = \frac{\partial \mathbf{x}}{\partial \xi} = \mathbf{t} \tag{4}$$

The corresponding dual base vectors $\mathbf{G}^i$ and $\mathbf{g}^i$ are defined through the relationships $\mathbf{G}_i \cdot \mathbf{G}^j = \delta_i^j$ and $\mathbf{g}_i \cdot \mathbf{g}^j = \delta_i^j$, where δ_i^j is a Kronecker symbol. Note that $\mathbf{G}^3 = \mathbf{G}_3$. The identity tensor of the shell reference configuration (or the shell metric tensor) is $\mathbf{G} = \mathbf{G}_i \otimes \mathbf{G}^j = G_{ij}\mathbf{G}^i \otimes \mathbf{G}^j$, where $G_{ij} = \mathbf{G}_i \cdot \mathbf{G}_j$. The differential volume element is given as $dV = \sqrt{G} d\xi d\xi^1 d\xi^2$, where $\sqrt{G} = \mathbf{G}_3 \cdot (\mathbf{G}_1 \times \mathbf{G}_2)$.

The base vectors at the reference midsurface and at the deformed midsurface are obtained by setting $\xi = 0$ in (3) and (4), respectively, i.e. $\mathbf{A}_i = \mathbf{G}_i|_{\xi=0}$, and $\mathbf{a}_i = \mathbf{g}_i|_{\xi=0}$. For the reference configuration we have $\mathbf{A}_\alpha = \frac{\partial \boldsymbol{\varphi}_0}{\partial \xi^\alpha}$, $\mathbf{A}_3 = \mathbf{T}$. The corresponding dual base vectors of $\mathbf{A}_i$ and $\mathbf{a}_i$ are given as $\mathbf{A}_i \cdot \mathbf{A}^j = \delta_i^j$ and $\mathbf{a}_i \cdot \mathbf{a}^j = \delta_i^j$, respectively. Note that $\mathbf{A}^3 = \mathbf{A}_3$. The identity tensor of the shell reference midsurface (or the midsurface metric tensor) is $\mathbf{A} = \mathbf{A}_\alpha \otimes \mathbf{A}^\beta = A_{\alpha\beta}\mathbf{A}^\alpha \otimes \mathbf{A}^\beta$, where $A_{\alpha\beta} = \mathbf{A}_\alpha \cdot \mathbf{A}_\beta$, and the differential surface element is given as $dA = \sqrt{A} d\xi^1 d\xi^2$, where $\sqrt{A} = |\mathbf{A}_1 \times \mathbf{A}_2|$. We can further define a tensor, called shifter, which transforms the base vectors of the midsurface to the base vectors of the shell body. The shifter from the shell reference configuration, denoted as $\mathbf{Z}$, shifts $\mathbf{A}_i$ and $\mathbf{A}^i$ (defined at a midsurface point) to $\mathbf{G}_i$ and $\mathbf{G}^i$, respectively, i.e. $\mathbf{G}_i = \mathbf{Z}\mathbf{A}_i$ and $\mathbf{G}^i = \mathbf{Z}^{-T}\mathbf{A}^i$. The shifter $\mathbf{Z}$ is defined as $\mathbf{Z} = \mathbf{G}_i \otimes \mathbf{A}^i = \mathbf{A}_i \otimes \mathbf{A}^i + \xi \mathbf{T}_{,\alpha} \otimes \mathbf{A}^\beta = \mathbf{A} + \xi \mathbf{B}$, where $(\circ)_{,\alpha} = \frac{\partial (\circ)}{\partial \xi^\alpha}$, and $\mathbf{B}$ is the midsurface curvature tensor. Note, that $\mathbf{A} = (\mathbf{A}_i)_k \left(\mathbf{A}^i\right)_j \mathbf{e}_k \otimes \mathbf{e}_j = (\mathbf{A}_i)_k \left(\mathbf{A}^i\right)_k \mathbf{I} = \mathbf{I}$ and $\mathbf{A}_i \otimes \mathbf{A}^i = \mathbf{A}_\alpha \otimes \mathbf{A}^\alpha$.

Having defined base vectors and the shifter, we can proceed with the expression for the deformation gradient (here we use notation $\xi^3 = \xi$)

$$\mathbf{F} = \frac{\partial \mathbf{x}}{\partial \mathbf{X}} = \frac{\partial \mathbf{x}}{\partial \xi^i} \left[\frac{\partial \mathbf{X}}{\partial \xi^i}\right]^{-1} = \mathbf{g}_i \otimes \mathbf{G}^i \tag{5}$$

Knowing $\mathbf{F}$ we can obtain the components of the symmetric (displacement-compatible) Green-Lagrange strain tensor with respect to the convected basis $\mathbf{G}^i$

$$\begin{aligned} \mathbf{E}^u &= \frac{1}{2}\left(\mathbf{F}^T\mathbf{F} - \mathbf{G}\right) = \frac{1}{2}\left[\left(\mathbf{G}^i \otimes \mathbf{g}_i\right)\left(\mathbf{g}_j \otimes \mathbf{G}^j\right) - \mathbf{G}_i \cdot \mathbf{G}_j \left(\mathbf{G}^i \otimes \mathbf{G}^j\right)\right] \\ &= \frac{1}{2}\left(\mathbf{g}_i \cdot \mathbf{g}_j - \mathbf{G}_i \cdot \mathbf{G}_j\right)\mathbf{G}^i \otimes \mathbf{G}^j = E_{ij}^u \mathbf{G}^i \otimes \mathbf{G}^j \end{aligned} \tag{6}$$

By evaluation of dot products $\mathbf{g}_i \cdot \mathbf{g}_j$ and $\mathbf{G}_i \cdot \mathbf{G}_j$ in (6) one gets the strains E_{ij}^u varying quadratically with respect to the ξ coordinate

$$E_{ij}^u = \varepsilon_{ij}^u + \xi \kappa_{ij}^u + (\xi)^2 \eta_{ij}^u \tag{7}$$

where $\varepsilon_{33}^u = \kappa_{33}^u = \eta_{\alpha 3}^u = \eta_{3\alpha}^u = \eta_{33}^u = 0$. In this work we will truncate the strains $E_{\alpha\beta}^u$ after the linear term and the strains $E_{\alpha 3}^u = E_{3\alpha}^u$, after the constant term i.e.

$$E_{ij}^u \rightarrow \begin{cases} E_{\alpha\beta}^u \rightarrow E_{\alpha\beta}^u = \varepsilon_{\alpha\beta}^u + \xi \kappa_{\alpha\beta}^u \\ E_{\alpha 3}^u \rightarrow E_{\alpha 3}^u = \varepsilon_{\alpha 3}^u \qquad E_{3\alpha}^u = E_{\alpha 3}^u \end{cases} \tag{8}$$

Expressions for $\varepsilon_{\alpha\beta}^u$, $\kappa_{\alpha\beta}^u$ and $2\varepsilon_{\alpha 3}^u$ are the classical expressions for the shell membrane, the shell bending and the shell transverse shear strains, respectively, which are explicitly given as

$$\begin{aligned} \varepsilon_{\alpha\beta}^u &= \frac{1}{2}\left(\boldsymbol{\varphi}_{,\alpha} \cdot \boldsymbol{\varphi}_{,\beta} - \boldsymbol{\varphi}_{0,\alpha} \cdot \boldsymbol{\varphi}_{0,\beta}\right), \qquad 2\varepsilon_{\alpha 3}^u = \gamma_{\alpha 3}^u = \boldsymbol{\varphi}_{,\alpha} \cdot \mathbf{t} - \underbrace{\boldsymbol{\varphi}_{0,\alpha} \cdot \mathbf{T}}_{0} \\ \kappa_{\alpha\beta}^u &= \frac{1}{2}\left(\boldsymbol{\varphi}_{,\alpha} \cdot \mathbf{t}_{,\beta} + \boldsymbol{\varphi}_{,\beta} \cdot \mathbf{t}_{,\alpha} - \boldsymbol{\varphi}_{0,\alpha} \cdot \mathbf{T}_{,\beta} - \boldsymbol{\varphi}_{0,\beta} \cdot \mathbf{T}_{,\alpha}\right) = \boldsymbol{\varphi}_{,\alpha} \cdot \mathbf{t}_{,\beta} - \boldsymbol{\varphi}_{0,\alpha} \cdot \mathbf{T}_{,\beta} \end{aligned} \tag{9}$$

By using shifter, the strain tensor $\mathbf{E}^u$ from (6) can be transformed to the midsurface strain tensor object $\widehat{\mathbf{E}}^u$ as $\mathbf{E}^u = \mathbf{Z}^{-T}\widehat{\mathbf{E}}^u\mathbf{Z}^{-1}$, $\widehat{\mathbf{E}}^u = E^u_{ij}\mathbf{A}^i \otimes \mathbf{A}^j$. According to (8) the strain tensor $\widehat{\mathbf{E}}^u$ can be written as

$$\widehat{\mathbf{E}}^u = \varepsilon^u_{\alpha\beta}\mathbf{A}^\alpha \otimes \mathbf{A}^\beta + \varepsilon^u_{\alpha 3}\mathbf{A}^\alpha \otimes \mathbf{T} + \varepsilon^u_{3\beta}\mathbf{T} \otimes \mathbf{A}^\beta + \xi\kappa^u_{\alpha\beta}\mathbf{A}^\alpha \otimes \mathbf{A}^\beta \tag{10}$$

The stress tensor, which is conjugated with the Green Lagrange strain tensor $\mathbf{E}^u$, is the second Piola-Kirchhoff stress tensor $\mathbf{S}$. With respect to the basis $\mathbf{G}_i$ it can be expressed as $\mathbf{S} = S^{ij}\mathbf{G}_i \otimes \mathbf{G}_j$. By using shifter, one can have the midsurface stress tensor object $\widehat{\mathbf{S}}$ as $\mathbf{S} = \mathbf{Z}\widehat{\mathbf{S}}\mathbf{Z}^T$ and $\widehat{\mathbf{S}} = S^{ij}\mathbf{A}_i \otimes \mathbf{A}_j$.

2.2 Variational formulation. EAS functional

The starting point for the enhanced assumed strain (EAS) functional, which will provide basis for our finite element approximation, is the Hu-Washizu functional

$$\begin{aligned}\Pi_{HW}\left(\mathbf{u},\mathbf{t},E_{ij},S^{ij}\right) = &\int_A\int_{-h/2}^{h/2}\overline{W}\left(E_{ij},\circ\right)\mu d\xi dA \\ &+\int_A\int_{-h/2}^{h/2}S^{ij}\left(\underbrace{\left(\varepsilon^u_{ij}+\xi\kappa^u_{ij}\right)}_{E^u_{ij}(\mathbf{u},\mathbf{t})} - \underbrace{\left(\varepsilon_{ij}+\xi\kappa_{ij}\right)}_{E_{ij}}\right)\mu d\xi dA - \Pi_{ext}\end{aligned} \tag{11}$$

The independent functions in (11) are the midsurface displacement $\mathbf{u}$, the shell director position $\mathbf{t}$, the strain tensor $\mathbf{E}$ and the stress tensor $\mathbf{S}$. The displacement-compatible strain tensor $\mathbf{E}^u$ is expressed in terms of $\mathbf{u}$ and $\mathbf{t}$, i.e. $\mathbf{E}^u = \mathbf{E}^u\left(\mathbf{u},\mathbf{t}\right)$. The part of the functional, which is related to the prescribed load (and prescribed displacements and rotations), is also a function of $\mathbf{u}$ and $\mathbf{t}$, i.e. $\Pi_{ext} = \Pi_{ext}\left(\mathbf{u},\mathbf{t}\right)$. $\overline{W}$ is the strain energy function that depends on E_{ij} and midsurface geometry (metric tensor $\mathbf{A}$ and curvature tensor $\mathbf{B}$). The integration over the undeformed shell configuration in (11) is divided into the integration over the shell thickness and the integration over the midsurface $\int_V(\circ)\,dV = \int_A\int_{-h/2}^{h/2}(\circ)\,\mu d\xi dA$, where $\mu = \sqrt{G}/\sqrt{A}$ and $dA = \sqrt{A}d\mathcal{A}$. It can be shown that $\mathbf{S}\cdot(\mathbf{E}^u - \mathbf{E})$ equals to $\widehat{\mathbf{S}}\cdot\left(\widehat{\mathbf{E}}^u - \widehat{\mathbf{E}}\right)$.

It is assumed in (11) that the components of $\widehat{\mathbf{E}}$ with respect to the midsurface basis $\mathbf{A}^i$ (or equivalently, components of $\mathbf{E}$ with respect to the basis $\mathbf{G}^i$) are $E_{ij} = \varepsilon_{ij} + \xi\kappa_{ij}$, i.e. they have the same form as the displacement-compatible strain components (8). By introducing stress resultants

$$n^{ij} = \int_{-h/2}^{h/2}S^{ij}\mu d\xi, \qquad m^{ij} = \int_{-h/2}^{h/2}S^{ij}\xi\mu d\xi \tag{12}$$

and integrating strain energy function $\overline{W}$ across the thickness, one can rewrite (11) as

$$\begin{aligned}\Pi_{HW}\left(\mathbf{u},\mathbf{t},\varepsilon_{ij},\kappa_{ij},n^{ij},m^{ij}\right) = &\int_A W\left(\varepsilon_{ij},\kappa_{ij},\circ\right)dA \\ &-\int_A n^{ij}\left(\varepsilon_{ij}-\varepsilon^u_{ij}\right)dA - \int_A m^{ij}\left(\kappa_{ij}-\kappa^u_{ij}\right)dA - \Pi_{ext}\end{aligned} \tag{13}$$

Very often $\mathbf{Z}$ is set to $\mathbf{A}$ when integrating strain energy function for standard (relatively thin) shells. This is also the case for a simple strain resultant strain energy function that is used in this work

$$W = \frac{1}{2}\frac{Eh}{1-\nu^2}\varepsilon_{\alpha\beta}H^{\alpha\beta\gamma\delta}\varepsilon_{\gamma\delta} + \frac{1}{2}\frac{Eh^3}{12\left(1-\nu^2\right)}\kappa_{\alpha\beta}H^{\alpha\beta\gamma\delta}\kappa_{\gamma\delta} + \frac{1}{2}cGh\gamma_{\alpha 3}A^{\alpha\beta}\gamma_{\beta 3} \tag{14}$$

Here E is elastic modulus, ν is Poisson's ratio, $G = \frac{E}{2(1+\nu)}$ is shear modulus, c is shear correction factor, usually set to $c = 5/6$, $A^{\alpha\beta} = \mathbf{A}^\alpha\cdot\mathbf{A}^\beta$, and $H^{\alpha\beta\gamma\delta} = \nu A^{\alpha\beta}A^{\gamma\delta} + \frac{1}{2}\left(1-\nu\right)\left(A^{\alpha\gamma}A^{\beta\delta} + A^{\alpha\delta}A^{\beta\gamma}\right)$.

The crucial part of the enhanced assumed strain (EAS) method is an assumption that the strain tensor $\widehat{\mathbf{E}}$ is a sum of the displacement-compatible strain tensor $\widehat{\mathbf{E}}^u$, defined above, and an enhancing strain tensor $\widetilde{\mathbf{E}}$, i.e. $\widehat{\mathbf{E}} = \widehat{\mathbf{E}}^u + \widetilde{\mathbf{E}}$. In practice the enhancement is related to the strain components (9).

In this work we choose to make an enhancement of the membrane and the bending strain components, i.e.

$$\widetilde{\mathbf{E}} = \widetilde{\varepsilon}_{\alpha\beta}\mathbf{A}^{\alpha} \otimes \mathbf{A}^{\beta} + \xi\widetilde{\kappa}_{\alpha\beta}\mathbf{A}^{\alpha} \otimes \mathbf{A}^{\beta} \tag{15}$$

The components of the strain tensor are then

$$\varepsilon_{\alpha\beta} = \varepsilon^{u}_{\alpha\beta} + \widetilde{\varepsilon}_{\alpha\beta}, \qquad \kappa_{\alpha\beta} = \kappa^{u}_{\alpha\beta} + \widetilde{\kappa}_{\alpha\beta}, \qquad \gamma_{\alpha 3} = \gamma^{u}_{\alpha 3} \tag{16}$$

By inserting (16) in (13), a new functional is obtained which we call the EAS functional

$$\begin{aligned} \widehat{\Pi}_{EAS}\left(\mathbf{u}, \mathbf{t}, \widetilde{\varepsilon}_{ij}, \widetilde{\kappa}_{ij}, n^{ij}, m^{ij}\right) \;=\; & \int_A W\left(\varepsilon^{u}_{\alpha\beta} + \widetilde{\varepsilon}_{\alpha\beta}, \kappa^{u}_{\alpha\beta} + \widetilde{\kappa}_{\alpha\beta}, \gamma^{u}_{\alpha 3}\right) dA - \\ & \int_A n^{\alpha\beta}\widetilde{\varepsilon}_{\alpha\beta} dA - \int_A m^{\alpha\beta}\widetilde{\kappa}_{\alpha\beta} dA - \Pi_{ext} \end{aligned} \tag{17}$$

Introducing the variations for displacement $\mathbf{u} \to \mathbf{u} + \eta\delta\mathbf{u}$, shell director $\mathbf{t}\left(\boldsymbol{\vartheta}\right) \to \mathbf{t}\left(\boldsymbol{\vartheta} + \eta\delta\boldsymbol{\vartheta}\right)$, enhanced strains $\widetilde{\varepsilon}_{\alpha\beta} \to \widetilde{\varepsilon}_{\alpha\beta} + \eta\delta\widetilde{\varepsilon}_{\alpha\beta}$, $\widetilde{\kappa}_{\alpha\beta} \to \widetilde{\kappa}_{\alpha\beta} + \eta\delta\widetilde{\kappa}_{\alpha\beta}$, and stress resultants $n^{\alpha\beta} \to n^{\alpha\beta} + \delta n^{\alpha\beta}$, $m^{\alpha\beta} \to m^{\alpha\beta} + \delta m^{\alpha\beta}$ into (17), one can obtain the variation of (17) as $\delta\widehat{\Pi}_{EAS} = \frac{d\widehat{\Pi}_{EAS}}{d\eta}\mid_{\eta=0}$. At the stationary point $\delta\widehat{\Pi}_{EAS} = 0$ the equilibrium and kinematic relations are fulfilled in a weak form.

The next crucial assumption of the EAS method is the enforcement of the following orthogonality conditions

$$\int_A n^{\alpha\beta}\widetilde{\varepsilon}_{\alpha\beta} dA = 0, \qquad \int_A m^{\alpha\beta}\widetilde{\kappa}_{\alpha\beta} dA = 0 \tag{18}$$

The orthogonality conditions (18) simplify the EAS functional (17) and its variation $\delta\widehat{\Pi}_{EAS}$ to

$$\Pi_{EAS}\left(\mathbf{u}, \mathbf{t}, \widetilde{\varepsilon}_{ij}, \widetilde{\kappa}_{ij}\right) = \int_A W\left(\varepsilon^{u}_{\alpha\beta} + \widetilde{\varepsilon}_{\alpha\beta}, \kappa^{u}_{\alpha\beta} + \widetilde{\kappa}_{\alpha\beta}, \gamma^{u}_{\alpha 3}\right) dA - \Pi_{ext} \tag{19}$$

$$\begin{aligned} & \delta\Pi_{EAS}\left(\mathbf{u}, \mathbf{t}, \widetilde{\varepsilon}_{ij}, \widetilde{\kappa}_{ij}; \delta\mathbf{u}, \delta\mathbf{t}, \delta\widetilde{\varepsilon}_{ij}, \delta\widetilde{\kappa}_{ij}\right) \\ = \; & \int_A \left[\frac{\partial W}{\partial \varepsilon_{\alpha\beta}}\left(\delta\varepsilon^{u}_{\alpha\beta} + \delta\widetilde{\varepsilon}_{\alpha\beta}\right) + \frac{\partial W}{\partial \kappa_{\alpha\beta}}\left(\delta\kappa^{u}_{\alpha\beta} + \delta\widetilde{\kappa}_{\alpha\beta}\right) + q^{\alpha}\delta\gamma^{u}_{\alpha 3}\right] dA - \delta\Pi_{ext} \end{aligned} \tag{20}$$

where we defined the transverse shear forces as $q^{\alpha} = \frac{\partial W}{\partial \gamma_{\alpha 3}}$ and $\delta\Pi_{ext} = \frac{d}{d\eta}\Pi_{ext}(\mathbf{u} + \eta\delta\mathbf{u}, \mathbf{t}\left(\boldsymbol{\vartheta} + \eta\delta\boldsymbol{\vartheta}\right))\mid_{\eta=0}$. Note, that by enforcement of (18) we lose the device to obtain stress resultants $n^{\alpha\beta}$ and $m^{\alpha\beta}$, while the transverse shear stress resultants can be obtained through constitutive equation as $q^{\alpha} = \frac{\partial W}{\partial \gamma_{\alpha 3}}$.

By further introducing variation of (9) into (20), we can write $\delta\Pi_{EAS}$ as ($\delta\boldsymbol{\varphi} \equiv \delta\mathbf{u}$, see (2))

$$\delta\Pi_{EAS} = \int_A \left[\begin{array}{c} \frac{\partial W}{\partial \varepsilon_{\alpha\beta}}\left[\frac{1}{2}\left(\delta\boldsymbol{\varphi}_{,\alpha} \cdot \boldsymbol{\varphi}_{,\beta} + \boldsymbol{\varphi}_{,\alpha} \cdot \delta\boldsymbol{\varphi}_{,\beta}\right) + \delta\widetilde{\varepsilon}_{\alpha\beta}\right] + \\ \frac{\partial W}{\partial \kappa_{\alpha\beta}}\left(\delta\boldsymbol{\varphi}_{,\alpha} \cdot \mathbf{t}_{,\beta} + \boldsymbol{\varphi}_{,\alpha} \cdot \delta\mathbf{t}_{,\beta} + \delta\widetilde{\kappa}_{\alpha\beta}\right) + \\ q^{\alpha}\left(\delta\boldsymbol{\varphi}_{,\alpha} \cdot \mathbf{t} + \boldsymbol{\varphi}_{,\alpha} \cdot \delta\mathbf{t}\right) \end{array}\right] dA - \delta\Pi_{ext} \tag{21}$$

where $\delta\mathbf{t} = \frac{d}{d\eta}\mathbf{t}\left(\boldsymbol{\vartheta} + \eta\delta\boldsymbol{\vartheta}\right)\mid_{\eta=0}$ or $\delta\mathbf{t} = \mathcal{H}\delta\boldsymbol{\vartheta}$. Explicit form of $\mathcal{H}$ can be found in [7], [8], [13].

In solving equations (21) by the Newton iterative method, one makes use of the linearized form of (21), given as

$$Lin\left[\delta\Pi_{EAS}\left(\cdot\right)\right] = \delta\Pi_{EAS}\left(\cdot\right) + \Delta\delta\Pi_{EAS}\left(\cdot\right) = 0 \tag{22}$$

Linearization of $\delta\Pi_{EAS}$ at certain (fixed) values of $\mathbf{u}, \boldsymbol{\vartheta}$, $\widetilde{\varepsilon}_{\alpha\beta}$ and $\widetilde{\kappa}_{\alpha\beta}$ can be obtained in the following way. First we introduce the incrementation for the displacement $\mathbf{u} \to \mathbf{u} + \eta\Delta\mathbf{u}$, the shell director $\mathbf{t}\left(\boldsymbol{\vartheta}\right) \to \mathbf{t}\left(\boldsymbol{\vartheta} + \eta\Delta\boldsymbol{\vartheta}\right)$, the variation of the shell director $\delta\mathbf{t} \to \delta\mathbf{t}\left(\delta\boldsymbol{\vartheta}, \boldsymbol{\vartheta} + \eta\Delta\boldsymbol{\vartheta}\right)$, and the enhanced strains $\widetilde{\varepsilon}_{\alpha\beta} \to \widetilde{\varepsilon}_{\alpha\beta} + \eta\Delta\widetilde{\varepsilon}_{\alpha\beta}$, $\widetilde{\kappa}_{\alpha\beta} \to \widetilde{\kappa}_{\alpha\beta} + \eta\Delta\widetilde{\kappa}_{\alpha\beta}$ into (21). Then we obtain $\Delta\delta\Pi_{EAS} = \frac{d\delta\Pi_{EAS}}{d\eta}\mid_{\eta=0}$.

2.3 Finite element approximation

Let the initial shell midsurface A be discretized by n_{el} nonoverlaping elements with n_{en} nodes such that $A \approx \bigcup_{e=1}^{n_{el}} A_e$. Over the element domain A_e the initial shell configuration (the midsurface and the shell director) are interpolated as

$$\boldsymbol{\varphi}_0\left(\xi^1,\xi^2\right)=\sum_{a=1}^{n_{en}} N_a\left(\xi^1,\xi^2\right)\boldsymbol{\varphi}_{0a}, \qquad \mathbf{T}\left(\xi^1,\xi^2\right)=\sum_{a=1}^{n_{en}} N_a\left(\xi^1,\xi^2\right)\mathbf{T}_a \tag{23}$$

where $(\circ)_a$ are the corresponding nodal values. In this work we choose $n_{en}=4$ and the bi-linear shape functions $N_a\left(\xi^1,\xi^2\right)$, defined over the square domain $\mathcal{A}_e=[-1,1]\times[-1,1]$. Note, that $\mathbf{T}_a$ is chosen to coincide with the normal vector to a given shell midsurface at that nodal point. However, due to the bi-linear interpolation (23) $\mathbf{T}$ is only approximately perpendicular to the base vectors $\mathbf{A}_\alpha=\partial\boldsymbol{\varphi}_0/\partial\xi^\alpha$. The interpolation of the shell deformed configuration $\boldsymbol{\varphi}$, $\mathbf{t}$ is performed in a similar fashion as $\boldsymbol{\varphi}_0$, $\mathbf{T}$. The virtual quantities $\delta\boldsymbol{\varphi}$ and $\delta\mathbf{t}$ are interpolated in the same manner as $\boldsymbol{\varphi}$ and $\mathbf{t}$. Derivations of $\boldsymbol{\varphi}$, $\mathbf{t}$, $\delta\boldsymbol{\varphi}$ and $\delta\mathbf{t}$ with respect to ξ^α coordinates are obtained trivially. Linearization of $\boldsymbol{\varphi}$, $\mathbf{t}$, $\delta\boldsymbol{\varphi}$ and $\delta\mathbf{t}$ with respect to nodal values leads to

$$\Delta\boldsymbol{\varphi}\left(\xi^1,\xi^2\right)=\sum_{a=1}^{n_{en}} N_a\left(\xi^1,\xi^2\right)\Delta\boldsymbol{\varphi}_a, \qquad \Delta\mathbf{t}\left(\xi^1,\xi^2\right)=\sum_{a=1}^{n_{en}} N_a\left(\xi^1,\xi^2\right)\Delta\mathbf{t}_a$$

$$\Delta\delta\mathbf{t}\left(\xi^1,\xi^2\right)=\sum_{a=1}^{n_{en}} N_a\left(\xi^1,\xi^2\right)\Delta\delta\mathbf{t}_a \tag{24}$$

We note that $\Delta\delta\boldsymbol{\varphi}_a=\mathbf{0}$, and $\Delta\delta\mathbf{t}_a=\frac{d}{d\eta}\delta\mathbf{t}_a\left(\delta\boldsymbol{\vartheta}_a,\boldsymbol{\vartheta}_a+\eta\Delta\boldsymbol{\vartheta}_a\right)|_{\eta=0}=\delta\boldsymbol{\vartheta}_a^T\mathcal{S}_a\Delta\boldsymbol{\vartheta}_a$; see [7], [8], [13] for an explicit form of $\mathcal{S}_a$. Due to the above interpolations the linearization and the discretization are interchangeable. For that reason we can directly use (23)-(24) in (21) and (22) to obtain a system of finite element nonlinear equations and the corresponding finite element tangent stiffness matrix.

We can now proceed with the interpolation of the enhancing strains. Let $\widetilde{\Xi}^m_{\alpha\beta}$ and $\widetilde{\Xi}^b_{\alpha\beta}$ be the enhancing membrane and the enhancing bending strains, which we choose to be defined with respect to the basis $\mathbf{A}_0^\alpha$ at $\xi^1=\xi^2=0$. The choice of the constant element base is necessary in order to derive shell elements that are able to pass the patch test. Those strains can be transformed to $\widetilde{\varepsilon}_{\alpha\beta}$ and $\widetilde{\kappa}_{\alpha\beta}$ strains from (15) through relations

$$\widetilde{\Xi}^m_{\gamma\delta}\mathbf{A}_0^\gamma\otimes\mathbf{A}_0^\delta=\widetilde{\varepsilon}_{\alpha\beta}\mathbf{A}^\alpha\otimes\mathbf{A}^\beta, \qquad \widetilde{\Xi}^b_{\gamma\delta}\mathbf{A}_0^\gamma\otimes\mathbf{A}_0^\delta=\widetilde{\kappa}_{\alpha\beta}\mathbf{A}^\alpha\otimes\mathbf{A}^\beta \tag{25}$$

which lead to the transformation relations

$$\widetilde{\varepsilon}_{\alpha\beta}=\left(\mathbf{A}_\alpha\cdot\mathbf{A}_0^\gamma\right)\widetilde{\Xi}^m_{\gamma\delta}\left(\mathbf{A}_\beta\cdot\mathbf{A}_0^\delta\right), \qquad \widetilde{\kappa}_{\alpha\beta}=\left(\mathbf{A}_\alpha\cdot\mathbf{A}_0^\gamma\right)\widetilde{\Xi}^b_{\gamma\delta}\left(\mathbf{A}_\beta\cdot\mathbf{A}_0^\delta\right) \tag{26}$$

Let us now write the strains $\widetilde{\varepsilon}_{\alpha\beta}$ and $\widetilde{\kappa}_{\alpha\beta}$ as scalar products of two vectors, i.e.

$$\widetilde{\varepsilon}_{\alpha\beta}=\mathcal{G}_{\alpha\beta}\cdot\boldsymbol{\alpha}, \qquad \widetilde{\kappa}_{\alpha\beta}=\mathcal{G}_{\alpha\beta}\cdot\boldsymbol{\beta} \tag{27}$$

Vectors $\mathcal{G}_{\alpha\beta}$ include enhancing strains interpolation functions and transformation terms from (26), while vectors $\boldsymbol{\alpha}$ and $\boldsymbol{\beta}$ define parameters of enhancing strains. Explicit forms of those vectors will be discussed below in the next section. By introducing variations $\boldsymbol{\alpha}\rightarrow\boldsymbol{\alpha}+\eta\delta\boldsymbol{\alpha}$ and $\boldsymbol{\beta}\rightarrow\boldsymbol{\beta}+\eta\delta\boldsymbol{\beta}$, one can obtain the variation of (27) as $\delta\widetilde{\varepsilon}_{\alpha\beta}=\frac{d}{d\eta}\widetilde{\varepsilon}_{\alpha\beta}\left(\boldsymbol{\alpha}+\eta\delta\boldsymbol{\alpha}\right)|_{\eta=0}$ and $\delta\widetilde{\kappa}_{\alpha\beta}=\frac{d}{d\eta}\widetilde{\kappa}_{\alpha\beta}\left(\boldsymbol{\beta}+\eta\delta\boldsymbol{\beta}\right)|_{\eta=0}$, which leads to $\delta\widetilde{\varepsilon}_{\alpha\beta}=\mathcal{G}_{\alpha\beta}\cdot\delta\boldsymbol{\alpha}$, $\delta\widetilde{\kappa}_{\alpha\beta}=\mathcal{G}_{\alpha\beta}\cdot\delta\boldsymbol{\beta}$. Similarly, $\Delta\widetilde{\varepsilon}_{\alpha\beta}=\mathcal{G}_{\alpha\beta}\cdot\Delta\boldsymbol{\alpha}$ and $\Delta\widetilde{\kappa}_{\alpha\beta}=\mathcal{G}_{\alpha\beta}\cdot\Delta\boldsymbol{\beta}$.

One can now introduce the above interpolations into (21) in order to get a system of nonlinear equations. Each nodal or element variation defines one nonlinear equation. We get

$$\begin{aligned}
\delta\Pi_{EAS} \;=\;& \delta\boldsymbol{\varphi}_a\cdot\int_{A_e}\left[\frac{\partial W}{\partial\varepsilon_{\alpha\beta}}\left[\frac{1}{2}\left(N_{a,\alpha}\boldsymbol{\varphi}_{,\beta}+N_{a,\beta}\boldsymbol{\varphi}_{,\alpha}\right)\right]+\frac{\partial W}{\partial\kappa_{\alpha\beta}}\left(N_{a,\alpha}\mathbf{t}_{,\beta}\right)+q^\alpha\left(N_{a,\alpha}\mathbf{t}\right)\right]dA_e+\\
&\delta\mathbf{t}_a\cdot\int_{A_e}\left[\frac{\partial W}{\partial\kappa_{\alpha\beta}}\left(N_{a,\beta}\boldsymbol{\varphi}_{,\alpha}\right)+q^\alpha\left(N_a\boldsymbol{\varphi}_{,\alpha}\right)\right]dA_e+\\
&\delta\boldsymbol{\alpha}\cdot\int_{A_e}\left[\mathcal{G}_{\alpha\beta}\frac{\partial W}{\partial\varepsilon_{\alpha\beta}}\right]dA_e+\delta\boldsymbol{\beta}\cdot\int_{A_e}\left[\mathcal{G}_{\alpha\beta}\frac{\partial W}{\partial\kappa_{\alpha\beta}}\right]dA_e-\delta\Pi_{ext}=0
\end{aligned} \tag{28}$$

By defining $\delta\mathbf{x}_a = \left[\delta\boldsymbol{\varphi}_a^T, \delta\mathbf{t}_a^T\right]^T$ and $\delta\widehat{\boldsymbol{\alpha}} = \left[\delta\boldsymbol{\alpha}^T, \delta\boldsymbol{\beta}^T\right]^T$, eq. (28) can be written as

$$\delta\Pi_{EAS} = \delta\mathbf{x}_a \cdot \mathbf{f}_{a,int} + \delta\widehat{\boldsymbol{\alpha}} \cdot \mathbf{f}_{EAS} - \underbrace{\delta\mathbf{x}_a \cdot \mathbf{f}_{a,ext}}_{\delta\Pi_{ext}} = 0 \tag{29}$$

Linearization of $\delta\Pi_{EAS}$ (28) can be obtained by introducing the above interpolations into $\Delta\delta\Pi_{EAS}$, see (22). One gets

$$\begin{aligned}
\delta\mathbf{x}_a^T\mathbf{K}_{ab}\Delta\mathbf{x}_b &= \int_{A_e} \begin{bmatrix} \delta\boldsymbol{\varphi}_a \cdot \frac{1}{2}\left(N_{a,\alpha}\boldsymbol{\varphi}_{,\beta} + N_{a,\beta}\boldsymbol{\varphi}_{,\alpha}\right) \frac{\partial^2 W}{\partial\varepsilon_{\alpha\beta}\partial\varepsilon_{\gamma\delta}} \frac{1}{2}\left(N_{b,\gamma}\boldsymbol{\varphi}_{,\delta} + N_{b,\delta}\boldsymbol{\varphi}_{,\gamma}\right) \cdot \Delta\boldsymbol{\varphi}_b \\ \delta\boldsymbol{\varphi}_a \cdot \left(N_{a,\alpha}\mathbf{t}_{,\beta}\right) \frac{\partial^2 W}{\partial\kappa_{\alpha\beta}\partial\kappa_{\gamma\delta}} \left[\left(N_{b,\gamma}\mathbf{t}_{,\delta}\right) \cdot \Delta\boldsymbol{\varphi}_b + \left(N_{b,\delta}\boldsymbol{\varphi}_{,\gamma}\right) \cdot \Delta\mathbf{t}_b\right] + \\ \delta\mathbf{t}_a \cdot \left(N_{a,\beta}\boldsymbol{\varphi}_{,\alpha}\right) \frac{\partial^2 W}{\partial\kappa_{\alpha\beta}\partial\kappa_{\gamma\delta}} \left[\left(N_{b,\gamma}\mathbf{t}_{,\delta}\right) \cdot \Delta\boldsymbol{\varphi}_b + \left(N_{b,\delta}\boldsymbol{\varphi}_{,\gamma}\right) \cdot \Delta\mathbf{t}_b\right] + \\ \delta\boldsymbol{\varphi}_a \cdot \left(N_{a,\alpha}\mathbf{t}\right) \frac{\partial^2 W}{\partial\gamma_{\alpha 3}\partial\gamma_{\beta 3}} \left[\left(N_{b,\beta}\mathbf{t}\right) \cdot \Delta\boldsymbol{\varphi}_b + \left(N_b\boldsymbol{\varphi}_{,\beta}\right) \cdot \Delta\mathbf{t}_b\right] + \\ \delta\mathbf{t}_a \cdot \left(N_a\boldsymbol{\varphi}_{,\alpha}\right) \frac{\partial^2 W}{\partial\gamma_{\alpha 3}\partial\gamma_{\beta 3}} \left[\left(N_{b,\beta}\mathbf{t}\right) \cdot \Delta\boldsymbol{\varphi}_b + \left(N_b\boldsymbol{\varphi}_{,\beta}\right) \cdot \Delta\mathbf{t}_b\right] \end{bmatrix} dA_e + \\
&\int_{A_e} \begin{bmatrix} \frac{\partial W}{\partial\varepsilon_{\alpha\beta}} \frac{1}{2}\left[\delta\boldsymbol{\varphi}_a \cdot \left(N_{a,\alpha}N_{b,\beta}\right)\Delta\boldsymbol{\varphi}_b + \delta\boldsymbol{\varphi}_a \cdot \left(N_{a,\beta}N_{b,\alpha}\right)\Delta\boldsymbol{\varphi}_b\right] + \\ \frac{\partial W}{\partial\kappa_{\alpha\beta}} \left(\delta\boldsymbol{\varphi}_a \cdot \left(N_{a,\alpha}N_{b,\beta}\right)\Delta\mathbf{t}_b + \delta\mathbf{t}_a \cdot \left(N_{a,\beta}N_{b,\alpha}\right)\Delta\boldsymbol{\varphi}_b + N_{b,\beta}\boldsymbol{\varphi}_{,\alpha} \cdot \Delta\delta\mathbf{t}_b\right) + \\ q_\alpha \left(\delta\boldsymbol{\varphi}_a \cdot \left(N_{a,\alpha}N_b\right)\Delta\mathbf{t}_b + N_b\boldsymbol{\varphi}_{,\alpha} \cdot \Delta\delta\mathbf{t}_b\right) \end{bmatrix} dA_e \\
\delta\widehat{\boldsymbol{\alpha}}^T\overline{\mathbf{H}}_b\Delta\mathbf{x}_b &= \int_{A_e} \begin{bmatrix} \delta\boldsymbol{\alpha} \cdot \mathcal{G}_{\alpha\beta} \frac{\partial^2 W}{\partial\varepsilon_{\alpha\beta}\partial\varepsilon_{\gamma\delta}} \frac{1}{2}\left(N_{b,\gamma}\boldsymbol{\varphi}_{,\delta} + N_{b,\delta}\boldsymbol{\varphi}_{,\gamma}\right) \cdot \Delta\boldsymbol{\varphi}_b + \\ \delta\boldsymbol{\beta} \cdot \mathcal{G}_{\alpha\beta} \frac{\partial^2 W}{\partial\kappa_{\alpha\beta}\partial\kappa_{\gamma\delta}} \left[\left(N_{b,\gamma}\mathbf{t}_{,\delta}\right) \cdot \Delta\boldsymbol{\varphi}_b + \left(N_{b,\delta}\boldsymbol{\varphi}_{,\gamma}\right) \cdot \Delta\mathbf{t}_b\right] \end{bmatrix} dA_e \\
\delta\mathbf{x}_a^T\mathbf{H}_a\Delta\widehat{\boldsymbol{\alpha}} &= \int_{A_e} \begin{bmatrix} \delta\boldsymbol{\varphi}_a \cdot \frac{1}{2}\left(N_{a,\alpha}\boldsymbol{\varphi}_{,\beta} + N_{a,\beta}\boldsymbol{\varphi}_{,\alpha}\right) \frac{\partial^2 W}{\partial\varepsilon_{\alpha\beta}\partial\varepsilon_{\gamma\delta}} \mathcal{G}_{\gamma\delta} \cdot \Delta\boldsymbol{\alpha} + \\ \left[\delta\boldsymbol{\varphi}_a \cdot \left(N_{a,\alpha}\mathbf{t}_{,\beta}\right) + \delta\mathbf{t}_a \cdot \left(N_{a,\beta}\boldsymbol{\varphi}_{,\alpha}\right)\right] \frac{\partial^2 W}{\partial\kappa_{\alpha\beta}\partial\kappa_{\gamma\delta}} \mathcal{G}_{\gamma\delta} \cdot \Delta\boldsymbol{\beta} \end{bmatrix} dA_e \\
\delta\widehat{\boldsymbol{\alpha}}^T\mathbf{D}\Delta\widehat{\boldsymbol{\alpha}} &= \int_{A_e} \left[\delta\boldsymbol{\alpha} \cdot \mathcal{G}_{\alpha\beta} \frac{\partial^2 W}{\partial\varepsilon_{\alpha\beta}\partial\varepsilon_{\gamma\delta}} \mathcal{G}_{\gamma\delta} \cdot \Delta\boldsymbol{\alpha} + \delta\boldsymbol{\beta} \cdot \mathcal{G}_{\alpha\beta} \frac{\partial^2 W}{\partial\kappa_{\alpha\beta}\partial\kappa_{\gamma\delta}} \mathcal{G}_{\gamma\delta} \cdot \Delta\boldsymbol{\beta}\right] dA_e
\end{aligned} \tag{30, 31}$$

where $\Delta\mathbf{x}_b = \left[\Delta\boldsymbol{\varphi}_b^T, \Delta\mathbf{t}_b^T\right]^T$ and $\Delta\widehat{\boldsymbol{\alpha}} = \left[\Delta\boldsymbol{\alpha}^T, \Delta\boldsymbol{\beta}^T\right]^T$. From the first integral in (30) and the integrals in (31) the material part of the tangent stiffness matrix arises, while from the second integral in (30) one can get the geometric part of the tangent stiffness matrix. We note that the enhancement of strains influences only the material part, while the geometric part remains unchanged.

Discretized form of equation (22) now turns, for one element (e), into the following system of equations

$$\begin{bmatrix} \mathbf{K}^{(e)} & \mathbf{H}^{(e)} \\ \mathbf{H}^{(e)T} & \mathbf{D}^{(e)} \end{bmatrix} \begin{Bmatrix} \Delta\mathbf{x}^{(e)} \\ \Delta\widehat{\boldsymbol{\alpha}}^{(e)} \end{Bmatrix} = \begin{Bmatrix} \mathbf{f}_{ext}^{(e)} - \mathbf{f}_{int}^{(e)} \\ -\mathbf{f}_{EAS}^{(e)} \end{Bmatrix} \tag{32}$$

where

$$\mathbf{K}^{(e)} = \left[\mathbf{K}_{ab}\right], \quad \mathbf{H}^{(e)} = \left\{\mathbf{H}_a\right\}^T, \quad \Delta\mathbf{x}^{(e)} = \left\{\Delta\mathbf{x}_a^T\right\}^T, \quad \mathbf{f}_{ext}^{(e)} = \left\{\mathbf{f}_{a,ext}^T\right\}^T, \quad \mathbf{f}_{int}^{(e)} = \left\{\mathbf{f}_{a,int}^T\right\}^T \tag{33}$$

Note that $\Delta\widehat{\boldsymbol{\alpha}}^{(e)} = \Delta\widehat{\boldsymbol{\alpha}}$, and that $\mathbf{f}_{EAS}^{(e)}$ follows from (28). Explicit forms of $\mathbf{K}_{ab}$, $\mathbf{D}^{(e)}$ and $\mathbf{H}_a = \overline{\mathbf{H}}_a^T$ follow from (30) and (31). If enhancing strains are chosen to be discontinuous across the element boundaries, it is possible to eliminate the EAS parameters on the element level, before assembling the element matrices into the global matrices. From (32) one gets

$$\Delta\widehat{\boldsymbol{\alpha}}^{(e)} = -\mathbf{D}^{(e)-1}\left(\mathbf{H}^{(e)T}\Delta\mathbf{x}^{(e)} + \mathbf{f}_{EAS}^{(e)}\right) \tag{34}$$

By substituting (34) into (32) we obtain the following equations

$$\left(\mathbf{K}^{(e)} - \mathbf{H}^{(e)}\mathbf{D}^{(e)-1}\mathbf{H}^{(e)T}\right)\Delta\mathbf{x}^{(e)} = \mathbf{f}_{ext}^{(e)} - \mathbf{f}_{int}^{(e)} + \mathbf{H}^{(e)}\mathbf{D}^{(e)-1}\mathbf{f}_{EAS}^{(e)} \tag{35}$$

From (35) follows the condensed symmetric tangent element stiffness matrix and the element residuals vector

$$\mathbf{k}_T^{(e)} = \mathbf{K}^{(e)} - \mathbf{H}^{(e)}\mathbf{D}^{(e)-1}\mathbf{H}^{(e)T}, \qquad \mathbf{r}^{(e)} = \left\{\mathbf{f}_{ext}^{(e)} - \mathbf{f}_{int}^{(e)} + \mathbf{H}^{(e)}\mathbf{D}^{(e)-1}\mathbf{f}_{EAS}^{(e)}\right\} \tag{36}$$

Assembly of the element stiffness matrices $\mathbf{K}_T = \bigwedge_{e=1}^{n_{el}} \mathbf{k}_T^{(e)}$ and the element residual vectors $\mathbf{R} = \bigwedge_{e=1}^{n_{el}} \mathbf{r}^{(e)}$ leads to the global system of equations $\mathbf{K}_T\Delta\mathbf{x} = \mathbf{R}$, where $\Delta\mathbf{x} = \bigwedge_{e=1}^{n_{el}} \Delta\mathbf{x}^{(e)}$ and $\bigwedge_{e=1}^{n_{el}}$ is the assembly operator.

3 Derived 4-node EAS-ANS shell elements

It can be seen from (21) that the enhancing strains can be interpolated element-wise, since the variation of EAS functional is free of derivatives of enhancing strains. Prior of choosing interpolation for the enhancing strains, one has to take a look at the displacement-compatible strains, since the enhancing strains should both enrich and decompose the displacement-compatible strains. For 4-node element ($n_{en} = 4$) the displacement-compatible membrane and bending strains, $\varepsilon^u_{\alpha\beta}$ and $\kappa^u_{\alpha\beta}$ respectively, involve the following functions in the finite element bi-unit space $\mathcal{A}_e = [-1,1] \times [-1,1]$

$$[\varepsilon^u_{11}, \varepsilon^u_{22}, 2\varepsilon^u_{12}]^T \in span\mathbf{Y}, \qquad [\kappa^u_{11}, \kappa^u_{22}, 2\kappa^u_{12}]^T \in span\mathbf{Y} \tag{37}$$

where

$$\mathbf{Y} = \begin{bmatrix} 1 & 0 & 0 & \xi^2 & 0 & 0 & 0 & \left(\xi^2\right)^2 & 0 & 0 \\ 0 & 1 & 0 & 0 & \xi^1 & 0 & 0 & 0 & \left(\xi^1\right)^2 & 0 \\ 0 & 0 & 1 & 0 & 0 & \xi^1 & \xi^2 & 0 & 0 & \xi^1\xi^2 \end{bmatrix} \tag{38}$$

The enhancing strains are then chosen on the basis of (38).

Let us now rearrange the enhancing strains introduced in (25) in the following two vectors

$$\widetilde{\boldsymbol{\Xi}}^m = \left[\widetilde{\Xi}^m_{11}, \widetilde{\Xi}^m_{22}, 2\widetilde{\Xi}^m_{12}\right]^T \qquad \widetilde{\boldsymbol{\Xi}}^b = \left[\widetilde{\Xi}^b_{11}, \widetilde{\Xi}^b_{22}, 2\widetilde{\Xi}^b_{12}\right]^T \tag{39}$$

Then we can write the enhancing membrane and bending strains in the finite element bi-unit space $\mathcal{A}_e$ as

$$\widetilde{\boldsymbol{\Xi}}^m = \boldsymbol{\Gamma}^m\boldsymbol{\alpha} \qquad \widetilde{\boldsymbol{\Xi}}^b = \boldsymbol{\Gamma}^b\boldsymbol{\beta} \tag{40}$$

where $\boldsymbol{\alpha}$ and $\boldsymbol{\beta}$ are the vectors that were already introduced in (25). They contain enhancing membrane strain parameters and enhancing bending parameters. Matrices $\boldsymbol{\Gamma}^m$ and $\boldsymbol{\Gamma}^b$ consist of interpolation functions for those parameters. We consider the following three possibilities:

(a) with 4 enhancing parameters for the membrane and 4 for the bending strains leading to

$$\begin{matrix} \boldsymbol{\alpha} = [\alpha_1, \alpha_2, \alpha_3, \alpha_4]^T \\ \boldsymbol{\beta} = [\beta_1, \beta_2, \beta_3, \beta_4]^T \end{matrix}, \qquad \boldsymbol{\Gamma}^m = \boldsymbol{\Gamma}^b = \frac{1}{\sqrt{A}} \begin{bmatrix} \xi^1 & 0 & 0 & 0 \\ 0 & \xi^2 & 0 & 0 \\ 0 & 0 & \xi^1 & \xi^2 \end{bmatrix} \tag{41}$$

(b) with 5 enhancing parameters for the membrane and 5 for the bending strains leading to

$$\begin{matrix} \boldsymbol{\alpha} = [\alpha_1, \alpha_2, \alpha_3, \alpha_4, \alpha_5]^T \\ \boldsymbol{\beta} = [\beta_1, \beta_2, \beta_3, \beta_4, \beta_5]^T \end{matrix}, \qquad \boldsymbol{\Gamma}^m = \boldsymbol{\Gamma}^b = \frac{1}{\sqrt{A}} \begin{bmatrix} \xi^1 & 0 & 0 & 0 & 0 \\ 0 & \xi^2 & 0 & 0 & 0 \\ 0 & 0 & \xi^1 & \xi^2 & \xi^1\xi^2 \end{bmatrix} \tag{42}$$

(c) with 7 enhancing parameters for the membrane and 7 for the bending strains leading to

$$\begin{matrix} \boldsymbol{\alpha} = [\alpha_1, \alpha_2, \alpha_3, \alpha_4, \alpha_5, \alpha_6, \alpha_7]^T \\ \boldsymbol{\beta} = [\beta_1, \beta_2, \beta_3, \beta_4, \beta_5, \beta_6, \beta_7]^T \end{matrix}, \qquad \boldsymbol{\Gamma}^m = \boldsymbol{\Gamma}^b = \frac{1}{\sqrt{A}} \begin{bmatrix} \xi^1 & 0 & 0 & 0 & \xi^1\xi^2 & 0 & 0 \\ 0 & \xi^2 & 0 & 0 & 0 & \xi^1\xi^2 & 0 \\ 0 & 0 & \xi^1 & \xi^2 & 0 & 0 & \xi^1\xi^2 \end{bmatrix} \tag{43}$$

The transformation of the $\widetilde{\Xi}^m_{\alpha\beta}$ and $\widetilde{\Xi}^b_{\alpha\beta}$ strains to the $\widetilde{\varepsilon}_{\alpha\beta}$ and $\widetilde{\kappa}_{\alpha\beta}$ strains is obtained by using (26). By defining vectors

$$\widetilde{\boldsymbol{\varepsilon}} = [\widetilde{\varepsilon}_{11}, \widetilde{\varepsilon}_{22}, 2\widetilde{\varepsilon}_{12}]^T \qquad \widetilde{\boldsymbol{\kappa}} = [\widetilde{\kappa}_{11}, \widetilde{\kappa}_{22}, 2\widetilde{\kappa}_{12}]^T \tag{44}$$

the following matrix, see (26), can be obtained for the transformation of (39) into (44)

$$\mathbf{T} = \begin{bmatrix} \left(c^1_1\right)^2 & \left(c^2_1\right)^2 & 2c^1_1c^2_1 \\ \left(c^1_2\right)^2 & \left(c^2_2\right)^2 & 2c^1_2c^2_2 \\ 2c^1_2c^1_1 & 2c^2_1c^2_2 & 2c^1_1c^2_2 + 2c^2_1c^1_2 \end{bmatrix} \tag{45}$$

where $c^\gamma_\alpha = \mathbf{A}_\alpha \cdot \mathbf{A}^\gamma_0$. Finally, the enhancing strains can be given as

$$\widetilde{\boldsymbol{\varepsilon}} = \mathbf{T}\widetilde{\boldsymbol{\Xi}}^m = \mathbf{T}\boldsymbol{\Gamma}^m\boldsymbol{\alpha} = \left[\begin{array}{ccc} \mathcal{G}_{11}^T & \mathcal{G}_{22}^T & 2\mathcal{G}_{12}^T \end{array}\right]^T \boldsymbol{\alpha}, \quad \widetilde{\boldsymbol{\kappa}} = \mathbf{T}\widetilde{\boldsymbol{\Xi}}^b = \mathbf{T}\boldsymbol{\Gamma}^b\boldsymbol{\beta} = \left[\begin{array}{ccc} \mathcal{G}_{11}^T & \mathcal{G}_{22}^T & 2\mathcal{G}_{12}^T \end{array}\right]^T \boldsymbol{\beta} \tag{46}$$

where $[\mathcal{G}_{11}, \mathcal{G}_{22}, \mathcal{G}_{12} = \mathcal{G}_{21}] = (\mathbf{T}\boldsymbol{\Gamma}^m)^T = \left(\mathbf{T}\boldsymbol{\Gamma}^b\right)^T$.

Having defined interpolation of the enhancing strains, we proceed with the membrane forces and the bending moments. They can be defined with respect to the basis $\mathbf{A}_\alpha$ or to the basis $\mathbf{A}_{0,\alpha}$ at $\xi^1 = \xi^2 = 0$, i.e.

$$n^{\alpha\beta}\mathbf{A}_\alpha \otimes \mathbf{A}_\beta = N^{\alpha\beta}\mathbf{A}_{0,\alpha} \otimes \mathbf{A}_{0,\beta}, \quad m^{\alpha\beta}\mathbf{A}_\alpha \otimes \mathbf{A}_\beta = M^{\alpha\beta}\mathbf{A}_{0,\alpha} \otimes \mathbf{A}_{0,\beta} \tag{47}$$

From (47) the following rule is obtained for the transformation between the components

$$n^{\alpha\beta} = (\mathbf{A}^\alpha \cdot \mathbf{A}_{0,\gamma})\, N^{\gamma\delta} \left(\mathbf{A}^\beta \cdot \mathbf{A}_{0,\delta}\right), \quad m^{\alpha\beta} = (\mathbf{A}^\alpha \cdot \mathbf{A}_{0,\gamma})\, M^{\gamma\delta} \left(\mathbf{A}^\beta \cdot \mathbf{A}_{0,\delta}\right) \tag{48}$$

It can be now seen that the orthogonality condition $(18)_1$ is satisfied for constant forces $N^{\alpha\beta}$,since one can have from (48) and (26)

$$\begin{aligned} n^{\alpha\beta}\widetilde{\varepsilon}_{\alpha\beta}dA &= N^{\gamma\delta}\widetilde{\Xi}^m_{\gamma\delta}\mathbf{A}_0^{\gamma,T}\left(\mathbf{A}_\alpha \otimes \mathbf{A}^\alpha\right)\mathbf{A}_{0,\gamma}\mathbf{A}_0^{\delta,T}\left(\mathbf{A}_\beta \otimes \mathbf{A}^\beta\right)\mathbf{A}_{0,\delta} \\ &= N^{\gamma\delta}\widetilde{\Xi}^m_{\gamma\delta}\left(\mathbf{A}_0^\gamma \cdot \mathbf{A}_{0,\gamma}\right)\left(\mathbf{A}_0^\delta \cdot \mathbf{A}_{0,\delta}\right) = N^{\gamma\delta}\widetilde{\Xi}^m_{\gamma\delta} \end{aligned} \tag{49}$$

and, therefore,

$$\begin{aligned} \int_{A_e} n^{\alpha\beta}\widetilde{\varepsilon}_{\alpha\beta}dA &= \int_{\mathcal{A}_e} n^{\alpha\beta}\widetilde{\varepsilon}_{\alpha\beta}\sqrt{A}d\xi^1 d\xi^2 = \int_{\mathcal{A}_e} N^{\alpha\beta}\widetilde{\Xi}^m_{\alpha\beta}\sqrt{A}d\xi^1 d\xi^2 = N^{\alpha\beta}\int_{\mathcal{A}_e}\widetilde{\Xi}^m_{\alpha\beta}\sqrt{A}d\xi^1 d\xi^2 \\ &= \mathbf{N}_0^T\int_{\mathcal{A}_e}\widetilde{\boldsymbol{\Xi}}^m\sqrt{A}d\xi^1 d\xi^2 = \mathbf{N}_0^T\underbrace{\left(\int_{\mathcal{A}_e}\boldsymbol{\Gamma}^m\sqrt{A}d\xi^1 d\xi^2\right)}_{\mathbf{0},\text{ see (41)-(43)}}\boldsymbol{\alpha} = 0 \end{aligned} \tag{50}$$

where $\mathbf{N}_0^T = \left[N^{11}, N^{22}, N^{12}\right]$. Similar expression can be obtained for the orthogonality condition $(18)_2$ and constant moments $\mathbf{M}_0^T = \left[M^{11}, M^{22}, M^{12}\right]$. Thus, the orthogonality conditions (18) hold at least for constant membrane forces and bending moments. Therefore, the elements which define enhancing strains in a manner (41)-(43) pass the patch test. To fully satisfy orthogonality conditions (18) one should also carefully design the interpolation of stress resultants. However, one can choose a partial satisfaction of orthogonality conditions in the sense of (50), which does not force interpolation of stress resultants. As a consequence a device to compute stress resultants is lost. For postprocessing purposes the stress resultants are usually approximated as $n^{\alpha\beta} \approx \frac{\partial W}{\partial \varepsilon_{\alpha\beta}}$ and $m^{\alpha\beta} \approx \frac{\partial W}{\partial \kappa_{\alpha\beta}}$. Such an approach is also taken in this paper.

To avoid the transverse shear locking, the ANS concept is chosen. The transverse shear strain field over the 4-node shell element is given by ANS interpolation [2]. The transverse shear strains are evaluated, using $(9)_2$, only at element edge mid-points A, B, C and D, where $\boldsymbol{\varphi}_0^I = \frac{1}{2}\left(\boldsymbol{\varphi}_{0J} + \boldsymbol{\varphi}_{0K}\right)$, see (23), where $I = A, B, C, D$, $J = 1, 2, 3, 4$ and $K = 2, 3, 4, 1$. The interpolation across the element is further given as

$$\gamma_{13} = \frac{1}{2}\left(1 - \xi^2\right)\gamma_{13}^A + \frac{1}{2}\left(1 + \xi^2\right)\gamma_{13}^C, \quad \gamma_{23} = \frac{1}{2}\left(1 - \xi^1\right)\gamma_{23}^D + \frac{1}{2}\left(1 + \xi^1\right)\gamma_{23}^B \tag{51}$$

4 Numerical examples

The computer implementation of the elements from Table 1 is in accordance with the above derivation, except that the local Cartesian frames are introduced at the integration points to simplify implementation. The computer codes were generated by using symbolic code manipulation program AceGen [19], [18]. Those codes were introduced into the finite element analysis program AceFEM [19].

4.1 Path-independence test

In this example we test the derived nonlinear elastic shell elements for path-independency. The test is similar to that presented in Jabareen and Rubin [14] for nonlinear elastic solid elements. We consider a single square shell element with side length $a = 10$, thickness $h = 0.01$, and material constants $E = 10^4$, $\nu = 0.3$. It has two nodes fixed (both displacements and rotations are restrained), one node is free, and displacements of one node (labeled as 1) are prescribed. The node 1 is translated sequentually on 6 straight line segments (see Fig. 1). Displacements at the points A to F are defined as $\mathbf{u}_{1A} = [0, 0, \beta]^T$, $\mathbf{u}_{1B} = [0, -\beta, \beta]^T$, $\mathbf{u}_{1C} = [\beta, -\beta, \beta]^T$, $\mathbf{u}_{1D} = [\beta, -\beta, 0]^T$, $\mathbf{u}_{1E} = [\beta, 0, 0]^T$, $\mathbf{u}_{1F} = [0, 0, 0]^T$, where $\beta = 5$. Each segmental translation was analyzed by using 100 increments. One can calculate the total external work done on the element at a certain pseudo-time $\overline{t}$ as $W = \int_0^{\overline{t}} \mathbf{f}_1 \cdot \dot{\mathbf{u}}_1 dt$, where $\mathbf{f}_1$ is the external nodal force applied to node 1. The integral was calculated for the path ABC (one half of the cycle) and for the path $ABCDEF$ (full cycle) by using trapezoidal integration rule. The corresponding external work is denoted as W_{ABC} and W_{ABCDEF}, respectively. For hyperelastic elements the work of one cycle should be theoretically zero. Negative values would indicate that the element has generated energy, whereas positive values would indicate that the element has dissipated energy. Since the numerical error is always present the error of one cycle is defined as $E = W_{ABCDEF}/W_{ABC}$ to diminish its influence. The results in Table 2 indicate that all considered elements behave correctly and produce hyperelastic path-independent response.

4.2 Twisted beam

The twisted beam is clamped at one end and subjected to point forces at the middle of the other end, Fig 2. The twist angle is a linear function of x with value 0 at the clamped end and $\pi/2$ at the free end. Linear analysis is performed for forces $F_x = F_z = 0$, $F_y = 1$ and for two different thicknesses: $h = 0.32$ (data A) and $h = 0.05$ (data B). The remaining geometric, material and load characteristics are: width $w = 1.1$, length $l = 12$, and $E = 29 \times 10^6$, $\nu = 0.22$. Analytical value of displacement under the force in the y direction is 0.00174274 (data A), see [28], and 0.3427 (data B), see [21]. Normalized value of this displacement (with respect to analytical solution) is for derived elements presented in Table 3. It shows that M and MB elements give much better results that ANS element, and that the number of membrane and bending enhancing parameters practically does not influence the results. For nonlinear analysis data C is used: $w = 4.4$, $l = 12$, $h = 0.0032$, $E = 29 \times 10^6$, $\nu = 0.22$, Fig 2. The final values of applied forces are $F_x = 0$, $F_y = F_z = 0.04$. The displacement (in y direction) of the point of application of forces is presented in Fig. 3 as function of forces F_y and F_z. Similar conclusion as for the linear case can be made: M and MB elements give different results that ANS element (at the final load level the displacement of enhanced elements is approximately 4 times bigger then the displacement of ANS element), and the number of membrane and bending enhancing parameters is not important for this example.

4.3 Curved twisted beam

The curved twisted beam is clamped at one end and subjected to point forces at the middle of the other end, Fig. 4. The twist angle is a linear function of the arc-length s with value 0 at the clamped end and $\pi/2$ at the free end. Linear analysis is performed for width $w = 1.1$, radius $R = 5$, thickness $h = 0.32$, material constants $E = 29 \times 10^6$, $\nu = 0.22$, and $F_x = F_y = 0$, $F_z = 1$. Analytical solution for displacement under the force in z direction is 0.00626901, see [28]. Normalized value of this displacement (with respect to the analytical solution) is for derived elements presented in Table 4. It can be seen that the number of enhancing parameters has only marginal influence on results. For nonlinear analysis the following data is used $w = 4.4$, $R = 5$, $h = 0.32$, Fig. 4. The final value of forces are $F_x = F_y = 15 \times 10^3$, $F_z = 0$. The load factor versus displacement curves are given in Fig. 5 for 2×10 mesh. The curves of M and MB elements do not coincide with each other (as in the twisted beam example), although the difference between the minimum (M4) and the maximum (MB5) displacement at the final load level is rather small; around 3%. It is interesting to note that the ANS element is not exhibiting different behavior trend then M and MB elements, which is in contrast with the twisted beam example.

4.4 Half-sphere with a hole

This popular example is illustrated in Fig. 6 The data is: radius $r = 10$, thickness $h = 0.04$, $E = 6.825 \times 10^7$, $\nu = 0.3$, and the angle of the hole $\alpha = 18^o$. The results are presented in Fig. 7 (for 8×8 mesh) and Table 5. Considerable difference in results can be seen between ANS elements, M4 and MB4 elements on one hand and all the other elements on the other hand. It is interesting to see that M4 and MB4 elements show only small improvement with respect to the ANS elements, while others enhanced elements give considerably better results; see Table 5 where present results are compared with those reported in [25]. This may be due to the fact that the elements of the mesh are not planar; they are slightly warped. The interpolation of the enhanced in-plane shear thus becomes important. This example shows that 4 membrane enhancing parameters are sometimes not enough to improve the behavior of ANS elements. At least 5 membrane enhancing parameters are needed. On the other hand an inclusion of the bending parameters has, for this particular example, no effect in improvement of element performance.

4.5 Cylinder with free ends

A cylinder with length $L = 10.35$, radius $r = 4.953$, thickness $h = 0.094$, elastic modulus $E = 1.05\ 10^4$ and Poisson's ratio $\nu = 0.3125$ is pinched by two radially pulling forces P as shown in Fig. 8. Both ends of the cylinder are free. One quarter of the cylinder is discretized and the corresponding symmetry is taken into account. Two meshes, 4×16 and 8×32, are used. The meshes are structured and the elements are unwarped. The results are shown in Figs. 9 - 11, which present radial displacement of points A and B with respect to the magnitude of the applied forces. Results of M elements are compared in Figure 9, which shows that M4, M5 and M7 give practically identical results. Results of M and MB elements are compared in Figure 10, which again shows that MB4, MB5 and MB7 give almost identical results that are slightly different from those of M4, M5 and M7. Thus, in this example the bending enhancement parameters do have some (although small) influence on results. Finally, M5 and MB5 are compared in Fig. 11 for both meshes. For the finer mesh the difference between M5 and MB5 elements becomes negligible. We can conclude from this example that all M elements behave in a similar manner, that all MB elements behave in a similar manner, and that there is a small difference between results of M and MB elements for coarse meshes.

4.6 Cylinder with end diaphragms

The cylinder with radius $R = 100$, length $L = 200$, thickness $h = 1$, $E = 3 \times 10^4$, $\nu = 0.3$ has a rigid diaphragm at each end. Two radially pushing forces are acting at two points in the middle of the cylinder, see Fig. 12. The 8×16 mesh was used to discretize one quarter of the cylinder. The results are shown in Fig. 13. Several different curves are obtained, with M5 and M7 giving a single curve, and MB5 and MB7 giving another single curve. Several snap-throughs can be observed that are false and appear as a consequence of coarse mesh. Strain enhancement is unable to improve such false behavior, which is obvious, since strain enhancement is done only element-wise. On the other hand, the finer mesh 32×72 (not shown in figures) leads to one response curve for all elements and removes false buckling points in load-displacement curves. This example shows that a phenomena related to a coarse mesh, like e.g. false snap-through, cannot be avoided by using enhanced strain elements. It can be seen again from this example that for coarse meshes the bending enhancement parameters can have some, but rather small, influence on results.

5 Concluding remarks

In this work we derived several 4-node hyperelastic shell elements based on enhanced assumed strain (EAS) method (based on Green-Lagrange strains) and on assumed natural strain (ANS) method. The elements differ from each other on the number of the enhancing membrane and bending parameters. The elements are able to produce hyperelastic path-independent response. It can be conclude from the numerical examples that 4 membrane enhancing parameters are sometimes not enough to improve

performance of the standard ANS element, and that 7 membrane enhancing parameters are too many. It therefore seems that the optimal number of membrane enhancing parameters is 5. We can also conclude that an influence of the bending enhancement parameters on element performance is rather small.

We agree with the reviewer's remark that the above conclusions hold for isotropic elastic material models. For layered composite shells or for inelastic material models the influence of the membrane and bending EAS parameters on the computed response could have different character.

References

[1] Andelfinger U, Ramm E (1993) EAS-elements for two-dimensional, three-dimensional, plate and shell structures and their equivalence to HR-elements, Int J Numer Meth Engng 36:1311-1337

[2] Bathe KJ, Dvorkin E (1985) A four-node plate bending element based on Mindlin-Reissner plate theory and a mixed interpolation, Int J Numer Meth Engng 21:367-383

[3] Başar Y, Itskov M, Eckstein A (2000) Composite laminates: Nonlinear interlaminar stress analysis by multi-layer shell elements, Comput Methods Appl Mech Engrg 185:367-397

[4] Betsch P, Stein E (1996) A nonlinear extensible 4-node shell element based on continuum theory and assumed strain interpolations, J Nonlinear Sci 6:169-199

[5] Betsch P, Gruttmann F, Stein E (1996) A 4-node finite shell element for the implementation of general hyperelastic 3d-elasticity at finite strain, Comput Methods Appl Mech Engrg 130:57-79

[6] Bischoff M, Ramm E (1997) Shear deformable shell elements for large strains and rotations, Comput Methods Appl Mech Engrg 40:4427-4449

[7] Brank B, Perić D, Damjanić FB (1997) On large deformation of thin elasto-plastic shells: implementation of a finite rotation model for quadrilateral shell elements, Int J Numer Meth Engng 40:689-726

[8] Brank B, Ibrahimbegovic A (2001) On the relation between different parametrizations of finite rotations for shells, Engineering Computations 18:950-973

[9] Brank B, Korelc J, Ibrahimbegovic A (2002) Nonlinear shell problem formulation accounting for through-the-thickness stretching and its finite element implementation, Computers and Structures 80:699-717

[10] Büchter N, Ramm E, Roehl D (1994) Three-dimensional extension of nonlinear shell formulation based on the enhanced assumed strain concept, Int J Numer Meth Engng 37:2551–2568

[11] Eberlein R, Wriggers P (1999) Finite element concepts for finite elastoplastic strains and isotropic stress response in shells: theoretical and computational analysis, Comput Methods Appl Mech Engrg 171:243-279

[12] Gruttmann F, Wagner W (2006) Structural analysis of composite laminates using a mixed hybrid shell element, Comput Mech 37:479-497

[13] Ibrahimbegovic A, Brank B, Courtois P (2001) Stress resultant geometrically exact form of classical shell model and vector-like parametrization of constrained finite rotations, Int J Numer Meth Engng 52:1235–1252

[14] Jabareen M, Rubin MB (2007) Hyperelasticity and physical shear buckling of a block predicted by the Cosserat point element compared with inelasticity and hourglassing predicted by other element formulations, Comput Mech 40:447-459

[15] Kegl M, Brank B (2006) Shape optimization of truss-stiffened shell structures with variable thickness, Comput Methods Appl Mech Engrg 195:2611-2634

[16] Kegl M, Brank B, Harl B, Oblak MM (2007) Efficient handling of stability problems in shell optimization by asymmetric 'worst-case' shape imperfection, Int J Numer Meth Engng (in press)

[17] Klinkel S, Gruttmann F, Wagner W (1999) A continuum based three-dimensional shell element for laminated structures, Computers and Structures 71:43-62

[18] Korelc J (1997) Automatic generation of finite element code by simultaneous optimization of expressions, Theor Comput Sci 187:231-248

[19] Korelc J (2007) AceGen, AceFem, available at http://www.fgg.uni-lj.si/Symech

[20] Krätzig WB, Jun D (2003) On 'best' shell models - from classical shells, degenerated and multi-layered concepts to 3D, Archive of Applied Mechanics 73:1-25

[21] Parisch H (1991) An investigation of a finite rotaion four node assumed strain shell element, Int J Numer Meth Engng 31:127-150

[22] Sansour C, Kollmann FG (2000) Families of 4-node and 9-node finite elements for a finite deformation shell theory. An assessment of hybrid stress, hybrid strain and enhanced strain elements, Comput Mech 24: 435-447

[23] Simo JC, Rifai S (1990) A class of mixed assumed strain methods and the method of incompatible modes, Int J Numer Meth Engng 29:1595-1638

[24] Simo JC, Armero F (1992) Geometrically non-linear enhanced strain mixed methods and the method of incompatible modes, Int J Numer Meth Engng 33:1413-1449

[25] Sze KY, Liu XH, Lo SH (2004) Popular benchmark problems for geometric nonlinear analysis of shells, Finite Elements in Analysis and Design 40: 1551-1569

[26] Vu-Quoc L, Tan XG (2003) Optimal solid shells for non-linear analyses of multilayered composites. I. Statics, Comput Methods Appl Mech Engrg 192:975-1016

[27] Vu-Quoc L, Tan XG (2003) Optimal solid shells for non-linear analyses of multilayered composites. II. Dynamics, Comput Methods Appl Mech Engrg 192:1017-1059

[28] Zupan D, Saje M (2006) The linearized three-dimensional beam theory of naturally curved and twisted beams: The strain vector formulation, Comput Methods Appl Mech Engrg 195:4557-4578

Table 1: Derived EAS-ANS shell elements

Element	No. of membrane EAS parameters	No. of bending EAS parameters	ANS concept
ANS	0	0	Yes
M4	4	0	Yes
MB4	4	4	Yes
M5	5	0	Yes
MB5	5	5	Yes
M7	7	0	Yes
MB7	7	7	Yes

Table 2: Path-independence test: Error in the external work on a closed cycle

Element	ANS	M4	MB4	M5	MB5	M7	MB7
W_{ABC}	281.218	258.676	258.676	258.350	258.350	258.350	258.350
$E \times 10^{-6}$	1.45657	−7.46430	−7.46431	−6.29626	−6.29627	−6.29626	−6.29627

Table 3: Twisted beam.
Linear analysis. Normalized displacement under the force in y direction

Element	ANS	M4	MB4	M5	MB5	M7	MB7
2×6 (data A)	0.805484	0.955530	0.955587	0.955536	0.955593	0.955536	0.955593
2×6 (data B)	0.929200	0.933642	0.933723	0.933840	0.933919	0.933840	0.933919

Table 4: Curved twisted beam.
Linear analysis. Normalized displacement under the force in z direction

Element	ANS	M4	MB4	M5	MB5	M7	MB7
2×8	0.811193	0.837923	0.841945	0.838794	0.848457	0.838801	0.853834
4×12	0.894533	0.911465	0.914031	0.909376	0.914914	0.909376	0.917850
6×24	0.935155	0.941046	0.941106	0.939557	0.941211	0.939557	0.942801

Table 5: Half-sphere with a hole.
Radial displacements of points A and B at $F/2 = 100$. Mesh is 8×8 for one quarter of half-sphere

Element	ANS	M4	MB4	M5	MB5	M7	MB7	[25] (16×16)
U_A	2.871	2.894	2.898	3.181	3.185	3.181	3.185	3.406
$-U_B$	4.599	4.670	4.675	5.453	5.461	5.453	5.461	5.902

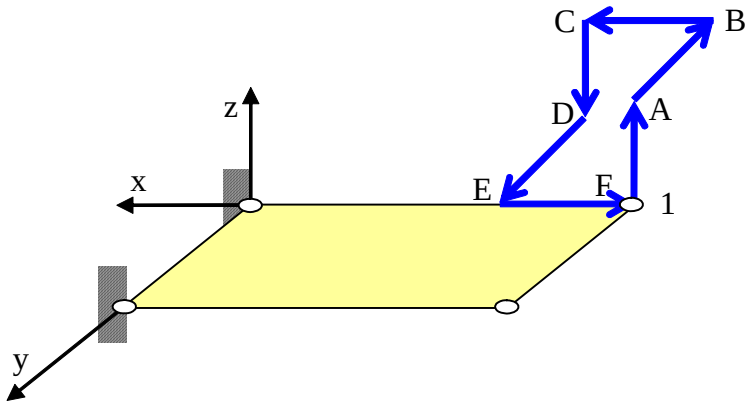

Figure 1: Path-independence test: Node 1 displacement path.

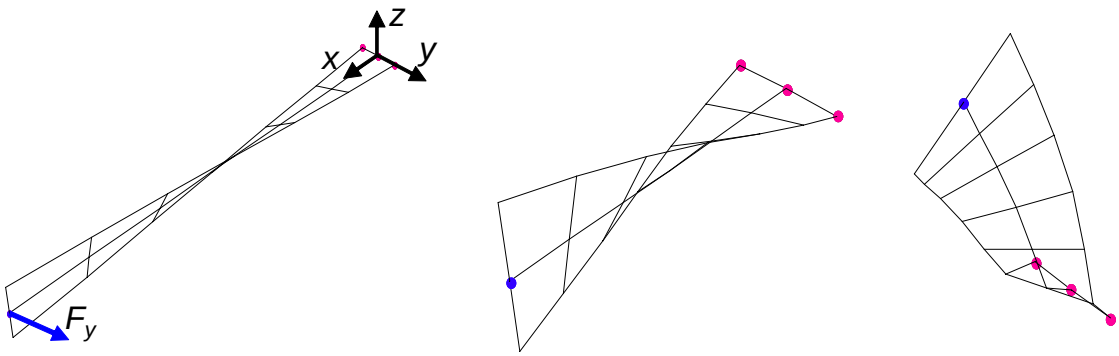

Figure 2: Twisted beam: (a) linear example, (b) nonlinear example, (c) deformed mesh for nonlinear example (M7) at $F_y = F_z = 0.036$ (mesh is 2×6)

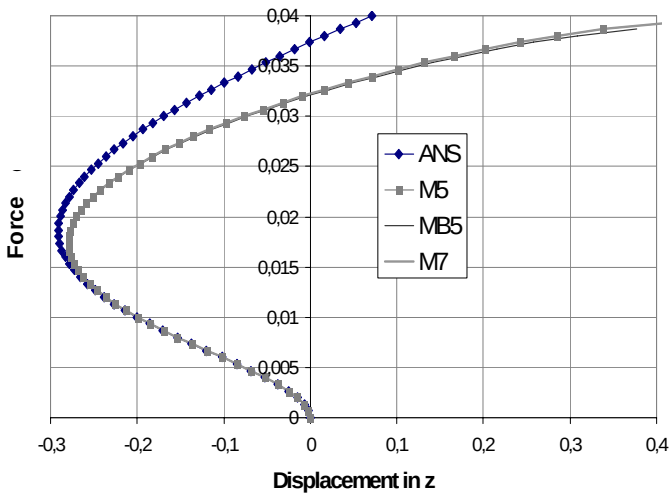

Figure 3: Twisted beam: Mesh is 2×6. Forces F_x and F_z versus y displacement of point under the forces

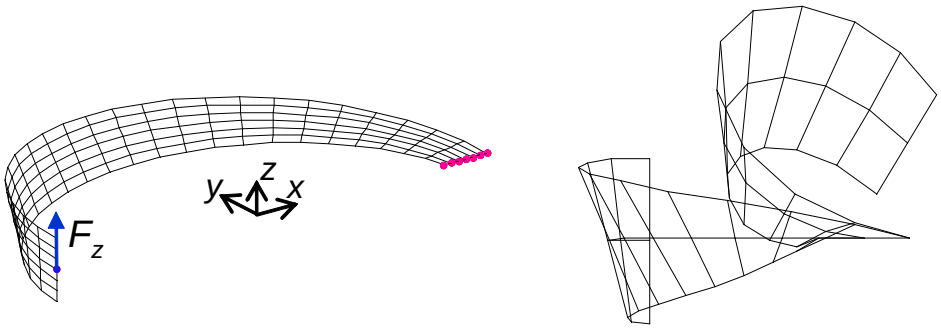

Figure 4: Curved twisted beam: (a) linear example, (b) initial and deformed mesh for nonlinear example (MB7, load factor is 1)

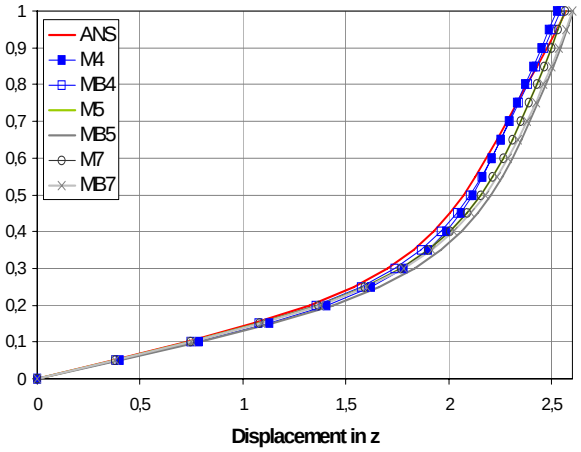

Figure 5: Curved twisted beam: Load factor versus z displacement curves. Mesh is 2×10

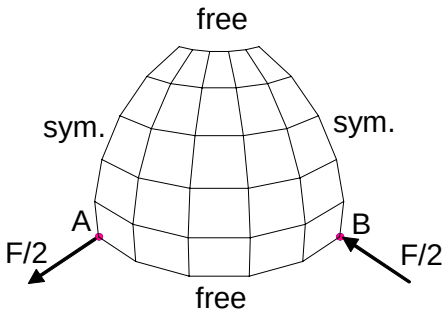

Figure 6: One quarter of half-sphere with 18^o hole discretized by 5×5 elements

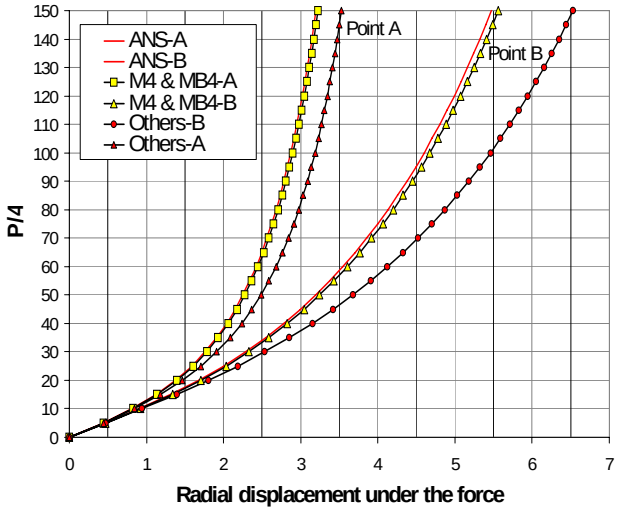

Figure 7: Half-sphere with a hole: Load-displacement curves. Mesh is 8×8.

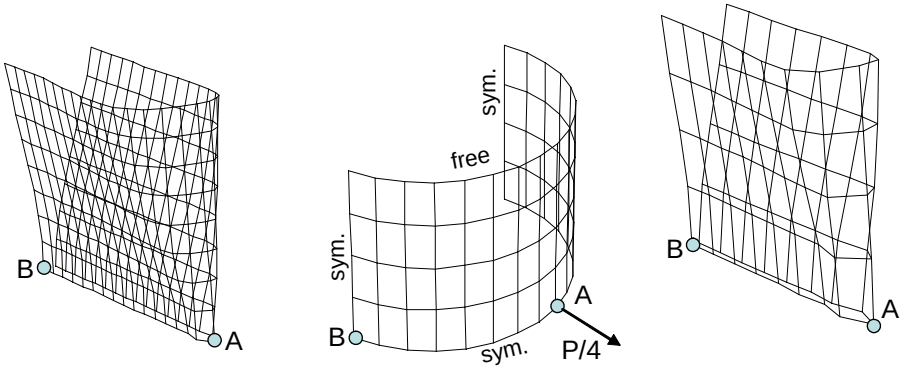

Figure 8: Cylinder with free ends subjected to radial pulling forces: (a) deformed 8×32 mesh (M5) at radial displacement of point A equal to 2.8, (b) problem description, (c) deformed 4×16 mesh (M5) at radial displacement of point A equal to 2.8

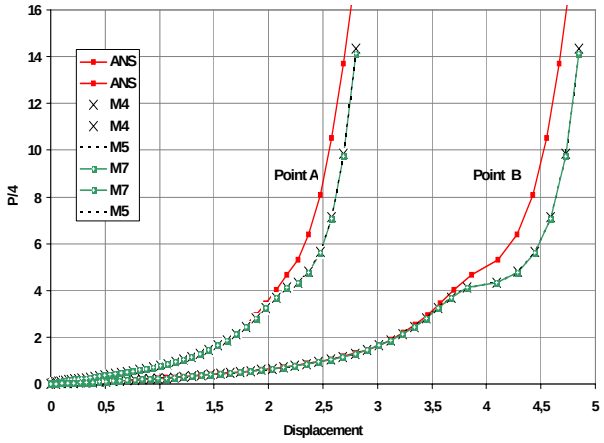

Figure 9: Cylinder with free ends: Load-displacement curves for points A and B; M elements; mesh is 4×16.

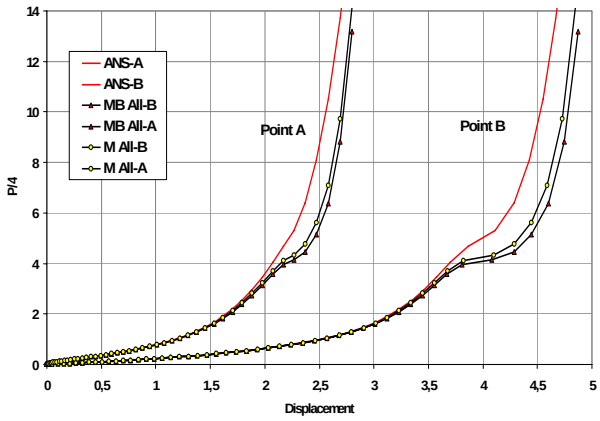

Figure 10: Cylinder with free ends: Load-displacement curves for points A and B; M and MB elements; mesh is 4×16.

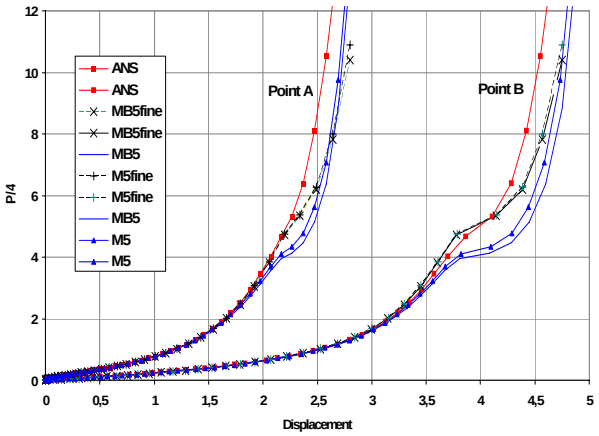

Figure 11: Cylinder with free ends: Load-displacement curves for points A and B; M and MB elements; meshes are 4×16 and 8×32 (fine).

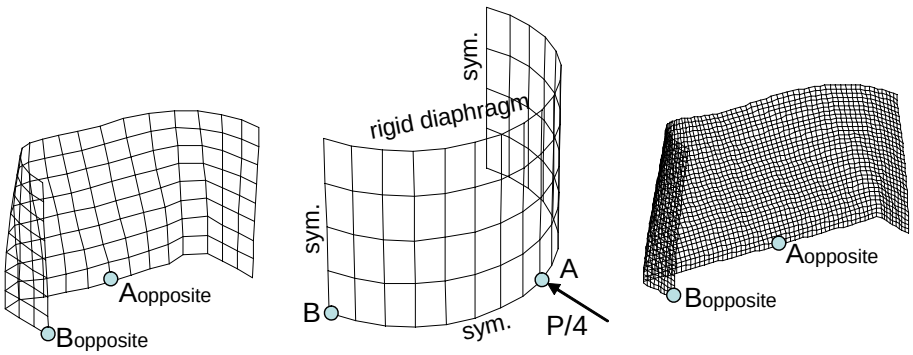

Figure 12: Cylinder with end diafragms: (a) deformed configuration (M5) for 8×16 mesh at radial displacement of point A equal to $0.45r$, (b) problem description, (c) deformed configuration (M5) for 32×72 mesh at radial displacement of point A equal to $0.6r$,

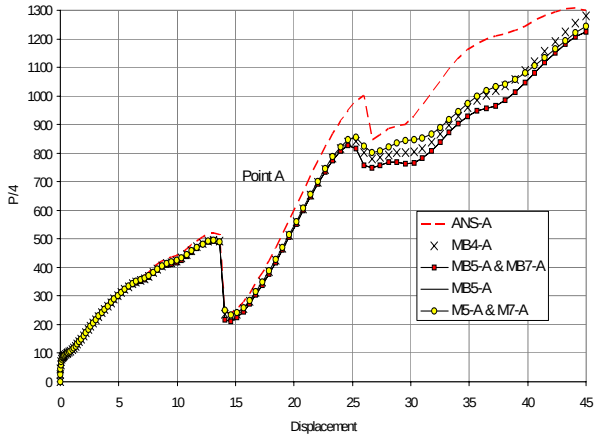

Figure 13: Cylinder with end diaphragms: Load-displacement curves for point A; mesh is 8×16.